Computers and Mathematics with Applications 59 (2010) 2403–2410

Contents lists available at ScienceDirect

Computers and Mathematics with Applications

journal homepage: www.elsevier.com/locate/camwa

Numerical simulation of sound generation in a mixing layer by the finite difference lattice Boltzmann method

Masayuki Hiraishi [a], Michihisa Tsutahara [b,*], R.C.K. Leung [c]

[a] *Graduate School of Science and Technology, Kobe University, Japan*

[b] *Graduate School of Engineering, Kobe University, Japan*

[c] *Department of Mechanical Engineering, Hong Kong Polytechnic University, Hong Kong, China*

ARTICLE INFO

Keywords:
Lattice Boltzmann method
Finite difference method
Computational aeroacoustics
Dispersion relation preserving scheme

ABSTRACT

We simulated aerodynamic sound in a two-dimensional mixing layer using the finite difference lattice Boltzmann method (FDLBM). We introduced a finite difference scheme, called the dispersion relation preserving (DRP) scheme, into the FDLBM to carry out an accurate simulation of aerodynamic problems. The scheme is designed such that the dispersion relation of the finite difference scheme is the same as that of the original partial differential equations and is useful for acoustic simulations. A turbulent flow field was simulated by large-eddy simulation (LES), using the Smagorinsky model, and the results were compared with those from a direct simulation based on the Navier–Stokes equations to confirm the usefulness of this method. The combination of the FDLBM and the DRP scheme was shown to be very effective for direct simulations of aerodynamic sound.

1. Introduction

In recent years, reduction of aerodynamic noise has become increasingly important subject. Numerical simulation of aerodynamic sound is an efficient method to simulate noise reduction; however, direct simulation of sound based on the Navier–Stokes equations is difficult because acoustic fluctuations are much smaller than those of fluid pressure, while the computational domain is very large. On the other hand, the finite difference lattice Boltzmann method (FDLBM) allows calculation of the acoustic field with higher accuracy and a lower calculation cost than other methods [1]. Though numerical simulation of turbulent flow by the FDLBM has been carried out [2], it is difficult to simulate acoustic fields generated by turbulent flow, because these acoustic fluctuations are damped by numerical viscosity [3]. To solve this problem, a highly accurate numerical scheme, called the dispersion relation preserving (DRP) scheme, was applied to the FDLBM. The purpose of this study is to simulate compressible turbulent flows with the FDLBM and estimate acoustic fields, because the effect of the turbulence cannot be neglected even for acoustic fields for high Reynolds number flows. We carried out large-eddy simulation (LES) of a two-dimensional mixing layer with the FDLBM using the Smagorinsky model.

2. The finite difference lattice Boltzmann method

2.1. Discrete BGK equation

In the FDLBM, the evolution of the density distribution function f_i for the particle velocity $c_{i\alpha}$ is governed by the following equation (the discrete BGK equation):

* Corresponding author.
E-mail addresses: hiraic@kobe-u.ac.jp (M. Hiraishi), tutahara@mech.kobe-u.ac.jp (M. Tsutahara).

0898-1221/$ – see front matter © 2009 Elsevier Ltd. All rights reserved.
doi:10.1016/j.camwa.2009.08.073

Table 1
Velocity set in 2D21V the model.

i	Velocity vector	$\|\mathbf{c}\|$
1	(0, 0)	0
2–5	(1, 0), (0, 1), (−1, 0), (0, −1)	1
6–9	(2, 0), (0, 2), (−2, 0), (0, −2)	2
10–13	(3, 0), (0, 3), (−3, 0), (0, −3)	3
14–17	(1, 1), (−1, 1), (−1, −1), (1, −1)	$\sqrt{2}$
18–21	(2, 2), (−2, 2), (−2, −2), (2, −2)	$2\sqrt{2}$

$$\frac{\partial f_i}{\partial t} + c_{i\alpha}\frac{\partial f_i}{\partial x_\alpha} - ac_{i\alpha}\frac{\partial}{\partial x_\alpha}\frac{f_i - f_i^{(0)}}{\tau} = -\frac{1}{\tau}(f_i - f_i^{(0)}) + \frac{F_\alpha(c_{i\alpha} - u_\alpha)}{(\gamma - 1)e} f_i^{(0)} \tag{1}$$

where the subscript i indicates the particle's direction. The subscript α indicates the x, y, and z components. $f_i^{(0)}$ is the local equilibrium distribution function, and τ is the relaxation parameter. The second term on the right-hand side is the external force term. Here F_α is the external force, u_α is the velocity, e is the internal energy, and γ is the specific heat ratio. The third term on the left-hand side is an additional term related to viscosity. The constant a ($\geq$0) is the coefficient of negative viscosity. The stability of the discrete BGK equation depends on the relaxation time, i.e., the time increment must be as small as the relaxation time. We can change the relationship between the kinetic viscosity and the relaxation parameter by adding this term. Then computational time can be shortened in high Reynolds number flows [4,5]. Additionally, we solve another BGK-type equation for the energy distribution function. In the lattice BGK model, the specific heat ratio is expressed by Eq. (2), which means that it can have a particular value that depends on the spatial dimension D.

$$\gamma = \frac{(D+2)}{D}. \tag{2}$$

To add an internal degree of freedom of energy, we introduce the energy distribution function g_i to represent energy modes, except the translation [4,6]. The energy distribution function is assumed to approach its local equilibrium state as the density distribution function f_i does:

$$\frac{\partial g_i}{\partial t} + c_{i\alpha}\frac{\partial g_i}{\partial x_\alpha} - ac_{i\alpha}\frac{\partial}{\partial x_\alpha}\frac{g_i - g_i^{(0)}}{\tau} = -\frac{1}{\tau}(g_i - g_i^{(0)}) + \frac{F_\alpha(c_{i\alpha} - u_\alpha)}{(\gamma - 1)e} g_i^{(0)}. \tag{3}$$

By introducing the energy distribution function, we can choose an arbitrary value for the specific heat ratio. The macroscopic variables (density, momentum, and internal energy) are defined as velocity moments of the distribution function:

$$\rho = \sum_i f_i \tag{4}$$

$$\rho u_\alpha = \sum_i f_i c_{i\alpha} \tag{5}$$

$$\frac{1}{2}\rho u^2 + \rho e = \sum_i \left(\frac{1}{2} f_i c_{i\alpha}^2 + g_i\right). \tag{6}$$

2.2. The local equilibrium distribution function

In the thermal fluid model of the FDLBM, the local equilibrium distribution function is defined as a third-order polynomial of velocity:

$$f_i^{(0)} = F_i\rho\left[1 - 2Bc_{i\alpha}u_\alpha + 2B^2(c_{i\alpha}u_\alpha)^2 + Bu^2 - \frac{4}{3}B^3(c_{i\alpha}u_\alpha)^3 - 2B^2c_{i\alpha}u_\alpha u^2\right] \tag{7}$$

$$g_i^{(0)} = Gf_i^{(0)} \tag{8}$$

$$G = \frac{D}{2}\left(\frac{D+2}{D} - \gamma\right)e \tag{9}$$

where D is the number of spatial dimensions and γ is the specific heat ratio. In this paper, we use a two-dimensional, 21 velocity model (D2Q21 model) as the discrete velocity model for thermal compressible flow. In prior simulations, the Aeolian tone emitted by a circular cylinder was successfully simulated using this model and the speed of sound for variable specific heat ratio is correctly recovered [4]. Fig. 1 and Tables 1 and 2 show the discrete velocity set and coefficients F_i and B in the D2Q21 model.

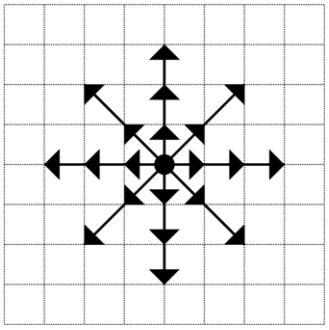

Fig. 1. Particle distribution in the D2Q21 model.

Table 2
Coefficients F_i and B in 2D21V model.

$i = 1$	$F_i = 1 + \frac{5}{4Bc^2}\left(\frac{17}{96B^2c^4} + \frac{35}{48Bc^2} + \frac{49}{45}\right)$
$i = 2$–5	$F_i = -\frac{1}{8Bc^2}\left(\frac{13}{16B^2c^4} + \frac{71}{24Bc^2} + 3\right)$
$i = 6$–9	$F_i = \frac{1}{16Bc^2}\left(\frac{5}{16B^2c^4} + \frac{25}{24Bc^2} + \frac{3}{5}\right)$
$i = 10$–13	$F_i = -\frac{1}{24Bc^2}\left(\frac{1}{16B^2c^4} + \frac{1}{8Bc^2} + \frac{1}{15}\right)$
$i = 14$–17	$F_i = \frac{1}{4B^3c^6}\left(\frac{Bc^2}{3} + \frac{1}{8}\right)$
$i = 18$–21	$F_i = -\frac{1}{1536B^3c^6}\left(2Bc^2 + 3\right)$
	$B = -\frac{1}{2(\gamma-1)e}$

2.3. Derivation of macroscopic equations

It can be shown that the Navier–Stokes equations can be derived from the discrete BGK Eq. (1) through a Chapman–Enskog expansion procedure [7]:

$$\frac{\partial \rho}{\partial t} + \frac{\partial \rho u_\alpha}{\partial x_\alpha} = 0 \tag{10}$$

$$\frac{\partial \rho u_\alpha}{\partial t} + \frac{\partial \rho u_\alpha u_\beta}{\partial x_\beta} = -\frac{\partial P}{\partial x_\alpha} + \frac{\partial}{\partial x_\beta}\mu\left(\frac{\partial u_\alpha}{\partial x_\beta} + \frac{\partial u_\beta}{\partial x_\alpha}\right) + \frac{\partial}{\partial x_\alpha}\left(\lambda\frac{\partial u_\beta}{\partial x_\beta}\right) + \rho F_\alpha \tag{11}$$

$$\begin{aligned}\frac{\partial}{\partial t}\rho\left(\frac{u^2}{2} + e\right) + \frac{\partial}{\partial x_\alpha}\left(\frac{u^2}{2} + e + \frac{P}{\rho}\right)\rho u_\alpha &= \frac{\partial}{\partial x_\alpha}\left(\kappa\frac{\partial e}{\partial x_\alpha}\right) + \frac{\partial}{\partial x_\alpha}\left[\mu u_\beta\left(\frac{\partial u_\alpha}{\partial x_\beta} + \frac{\partial u_\beta}{\partial x_\alpha}\right)\right] \\ &\quad + \frac{\partial}{\partial x_\alpha}\left(\lambda u_\alpha\frac{\partial u_\beta}{\partial x_\beta}\right) + \rho u_\alpha F_\alpha.\end{aligned} \tag{12}$$

The pressure P, the viscosity coefficient μ, the second viscosity coefficient λ, the heat conductivity κ, and the sound speed c_s have the following relations in the D2Q21 model:

$$P = (\gamma - 1)\rho e \tag{13}$$

$$\mu(= \rho\nu) = (\gamma - 1)\rho e(\tau - a) \tag{14}$$

$$\lambda = -(\gamma - 1)^2\rho e(\tau - a) \tag{15}$$

$$\kappa = 2\gamma\rho e(\tau - a) \tag{16}$$

$$c_s = \sqrt{\gamma(\gamma - 1)e}. \tag{17}$$

3. Dispersion relation preserving scheme

Direct simulation of an acoustic field requires an accurate scheme because acoustic fluctuations are much smaller than those of fluid pressure. Here, we use the dispersion relation preserving (DRP) scheme of Tam and Webb to discretize the convection terms [8,9]. This scheme possesses fourth-order accuracy with a 7-stencil:

$$\frac{\partial f_j}{\partial x} = \frac{1}{\Delta x}\sum_{l=-3}^{3} a_l f_{j+l} \tag{18}$$

where the coefficients a_l are chosen such that the effective wave number provided by the finite difference scheme is a close approximation to the actual wave number. To obtain an accurate numerical solution, it is necessary to eliminate the short wavelength spurious numerical waves. This can be done by introducing artificial selective damping terms in the finite difference equations.

$$\frac{\partial f_j}{\partial t} = \cdots - \frac{\nu_a}{(\Delta x)^2} \sum_{l=-3}^{3} d_l f_{j+l}. \tag{19}$$

The coefficient d_l is chosen to damp only the short waves, and not the long waves resolved accurately by the DRP scheme. The coefficient ν_a should be small enough to not damp acoustic fluctuations. In this study, ν_a is 10^{-4}.

4. Large-eddy simulation

4.1. FDLBM subgrid model

The basic principle of LES is that large-scale motions are resolved by the calculation and only unresolved small-scale motions need to be modeled. This requires a scale separation decomposing the unknowns into a local average $\bar{f}$ (large scale) and a subgrid-scale component f' (small scale), where $f = \bar{f} + f'$ stands for the instantaneous value of a quantity, by applying the filtering operation:

$$\bar{f}(t, x) = \int_{-\infty}^{\infty} G(t, y) f(x - y) \mathrm{d}y. \tag{20}$$

To transform the governing equation into one depending only on local averages, the filter operator is applied to the discrete BGK equation:

$$\frac{\partial \bar{f}_i}{\partial t} + c_{i\alpha} \frac{\partial \bar{f}_i}{\partial x_\alpha} - a c_{i\alpha} \frac{\partial}{\partial x_\alpha} \frac{\bar{f}_i - \bar{f}_i^{(0)}}{\tau_{\text{total}}} = -\frac{1}{\tau_{\text{total}}} (\bar{f}_i - \bar{f}_i^{(0)}) \tag{21}$$

where the relaxation parameter τ_{total} varies depending on time and space and shows the effects of the subgrid-scale component.

4.2. Smagorinsky model

We used the Smagorinsky model [10]. The Smagorinsky model is a subgrid-scale eddy viscosity model for incompressible flows, but it can work in low Mach number flows. Smagorinsky proposed the first subgrid-scale stress model. In this model, the anisotropic part of the subgrid-scale stress tensor takes the Boussinesq eddy viscosity form:

$$\tau_{\alpha\beta} - \frac{\delta_{\alpha\beta}}{3} \tau_{\gamma\gamma} = -2\nu_t \bar{S}_{\alpha\beta} \tag{22}$$

$$\tau_{\alpha\beta} = \overline{u_\alpha u_\beta} - \bar{u}_\alpha \bar{u}_\beta \tag{23}$$

$$\bar{S}_{\alpha\beta} = \frac{1}{2} \left(\frac{\partial u_\alpha}{\partial x_\beta} + \frac{\partial u_\beta}{\partial x_\alpha} - \frac{2}{3} \delta_{\alpha\beta} \frac{\partial u_\gamma}{\partial x_\gamma} \right) \tag{24}$$

where $\bar{S}_{\alpha\beta}$ is the strain tensor of the filtered velocity, ν_t is the subgrid eddy viscosity coefficient, and $\delta_{\alpha\beta}$ is the Kronecker delta. The subgrid eddy viscosity ν_t is

$$\nu_t = C \Delta^2 |\bar{S}|, \tag{25}$$

$$|\bar{S}| = \sqrt{2 \bar{S}_{\alpha\beta} \bar{S}_{\alpha\beta}}. \tag{26}$$

Here, C is the square of the Smagorinsky constant C_s. Δ is the filter width (grid size) and is taken to be the geometric average of the grid spacing in x and y directions, $\Delta = \sqrt{\Delta x \Delta y}$.

4.3. Employing the subgrid model for the FDLBM

When we employ the subgrid model for the FDLBM, we determine τ_{total} in the D2Q21 model as [11]

$$\nu_{\text{total}} = \nu + \nu_t = (\gamma - 1) e (\tau_{\text{total}} - a). \tag{27}$$

5. Simulation of the mixing layer

5.1. Problem description

We carried out LES of a two-dimensional mixing layer with the FDLBM using the Smagorinsky model. The longitudinal velocity profile of the mixing layer is given by the hyperbolic tangent shear layer profile:

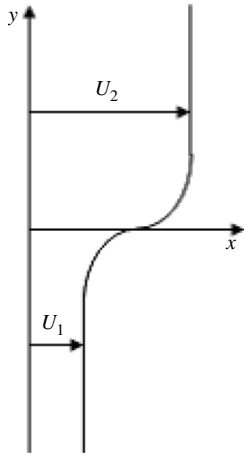

Fig. 2. Schematic diagram.

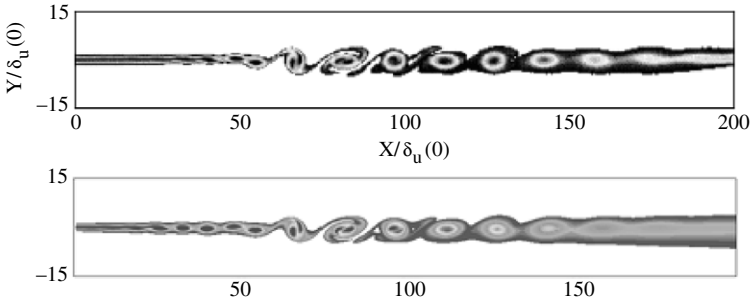

Fig. 3. Distribution of the vorticity.

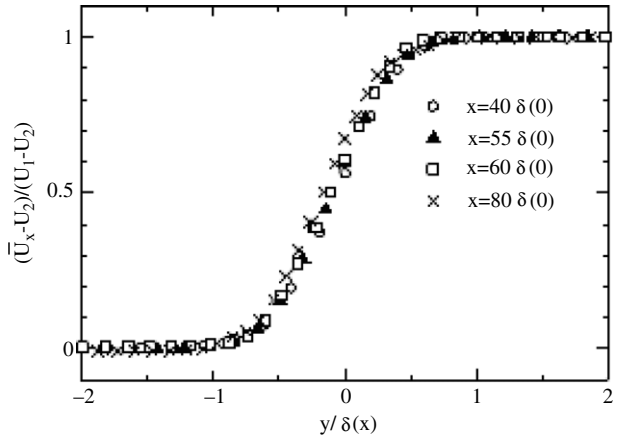

Fig. 4. Distribution of the mean velocity.

$$u_x(y) = \frac{U_1 + U_2}{2} + \frac{U_2 - U_1}{2} \tanh\left[\frac{2y}{\delta(0)}\right] \tag{28}$$

where $\delta(0)$ is the initial velocity thickness of the shear layer, and U_1 and U_2 are the velocities of the high-speed and low-speed streams, respectively. The Reynolds number, based on the initial velocity thickness, is $Re = \delta(0)(U_2 - U_1)/\nu = 1.28 \times 10^4$. The specific heat ratio is $\gamma = 1.4$. To control the vortex pairing in the mixing layer, the flow is excited by an external force. The coherent forcing for the shear layer was derived from the spatially evolving linear stability analysis of Michalke. The flow is forced at two frequencies, its fundamental frequency f_0 and first subharmonic frequency $f_0/2$ with a phase shift difference

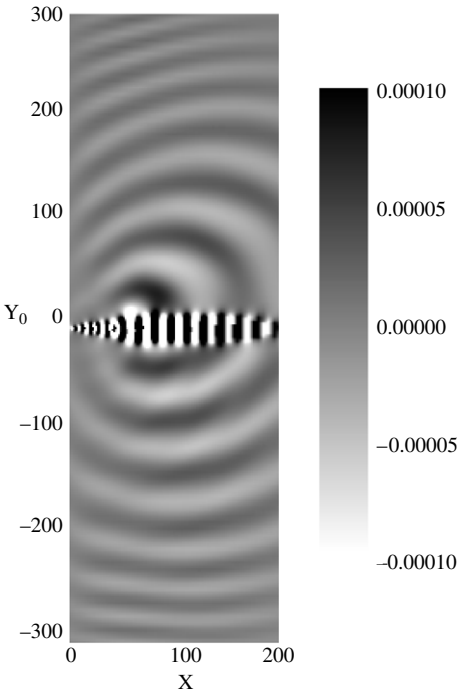

Fig. 5. Acoustic field.

of $\pi/2$ [12].

$$F_x = \frac{(y - y_0)}{\Delta y_0} E\left[\sin(2\pi f_0 t) + \cos(\pi f_0 t)\right] \tag{29}$$

$$F_y = \frac{(x - x_0)}{\Delta x_0} E\left[\sin(2\pi f_0 t) + \cos(\pi f_0 t)\right] \tag{30}$$

$$E = \epsilon \frac{U_1 + U_2}{2} \exp\left\{-\frac{\ln 2}{\Delta y_0^2}\left[(x - x_0)^2 + (y - y_0)^2\right]\right\}. \tag{31}$$

The coefficient ϵ is 5×10^{-4} for the fundamental frequency and 2.5×10^{-4} for the subharmonic frequency. The geometry of the computational domain is shown in Fig. 2. The flow is described in the Cartesian coordinate system x, y, in which the x-axis is aligned with the inflow direction, and the y-axis is perpendicular to x. The grid number is 441×441 and the minimum mesh size in longitudinal and lateral directions is $0.32\delta(0)$ and $0.16\delta(0)$, respectively. The grid points are concentrated in the shear zone. The scheme is explicit in time, and a second-order Runge–Kutta scheme is used. The shear layer velocity profile expressed by Eq. (28) is prescribed at the inlet boundary. Uniform flow is required at the longitudinal boundary. The convective outflow boundary condition is applied at the outflow boundary [13].

5.2. Numerical results

Fig. 3 shows the vorticity distribution near the mixing layer. The result of the FDLBM agrees well with the numerical result of DNS [14] and the experimental visualizations of Winant and Browand [15], i.e., vortex pairings occur at a fixed position around $x = 70\delta(0)$. The damping function is applied from $x = 130\delta(0)$; it dissipates vortices before other pairing happens downstream. There are then no secondary significant sound sources after the first pairing. Fig. 4 represents the distribution of the time-averaged longitudinal velocity $\bar{u}$. We confirm that the flow has self-similarity, which is a feature of the mixing layer flow. Fig. 5 shows the pressure distribution. We can confirm that acoustic waves radiate from the fixed point of vortex pairing. In the upper, high-speed flow, acoustic waves are affected by convection. Sound pressure directivity at a distance of $100\delta(0)$ from the noise source is shown in Fig. 6. The solid line and circles represent the results of DNS and the FDLBM, respectively. The result of the FDLBM agrees with that of DNS on acoustic directivity and the maximum value of the sound pressure level. However, they do not agree completely. It is assumed that this is caused by differences in the boundary conditions, i.e., a constant value is prescribed at the inlet and longitudinal boundary in this simulation, whereas the radiation boundary condition is applied in DNS. Fig. 7 represents the relationship between pressure and distance from the position of vortex pairing. According to theoretical prediction, the acoustic pressure decays in proportional to the distance to $-1/2$,

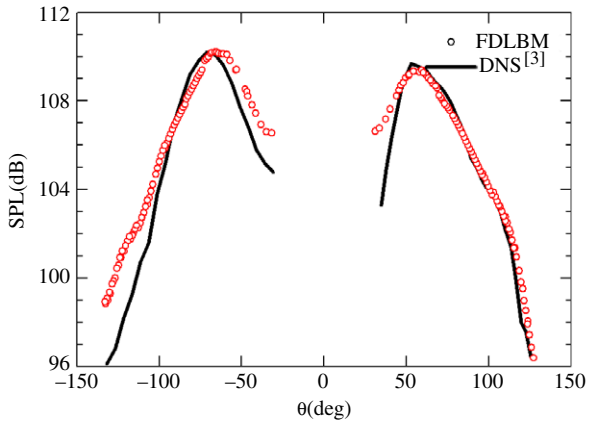

Fig. 6. Acoustic directivity.

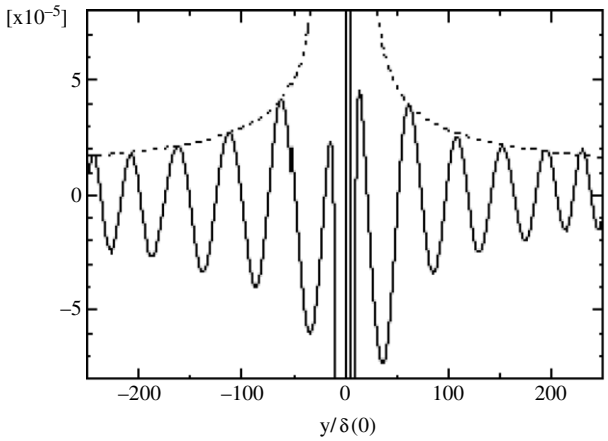

Fig. 7. Decay of the sound wave.

which is represented by the broken line. The solid lines show the acoustic pressure. The computational result agrees with the theoretical prediction.

6. Conclusions

We introduced the DRP scheme to the finite difference lattice Boltzmann compressible fluid model and simulated the sound generated in a mixing layer. Then these results were compared with numerical ones by direct simulation, based on the Navier–Stokes equations, to confirm the usefulness of this method. Numerical results from the FDLBM agree with the other results, i.e., vortex pairing in a mixing layer can be simulated correctly and the numerical result of sound pressure directivity has a good agreement with the other results. In conclusion, combining the FDLBM and DRP scheme is shown to be very effective for direct simulations of aerodynamic sound.

References

[1] M. Tsutahara, M. Kurita, T. Kataoka, Direct simulation of acoustic waves by the finite difference lattice Boltzmann method, Transactions of the Japan Society of Mechanical Engineers, Series B 69 (680) (2003) 89–95 (in Japanese).
[2] M. Hiraishi, M. Tsutahara, Application of dynamic Smagorinsky model to the finite difference lattice Boltzmann method, JSME Technical Journal (Journal of Fluid Science and Technology) 3 (1) (2008).
[3] M. Hiraishi, M. Tsutahara, Direct simulation of aerodynamic sound by the finite difference lattice Boltzmann method employing sub-grid model of turbulence, in: Proceedings of the 9th Western Pacific Acoustics Conference, CD-ROM, 2006.
[4] M. Tsutahara, T. Kataoka, K. Shikata, N. Takada, New model and scheme for compressible fluids of the finite difference lattice Boltzmann method and direct simulations of aerodynamic sound, Computers & Fluids 37 (2008) 79–89.
[5] M. Tsutahara, M. Kurita, T. Iwagami, A study of new finite difference lattice Boltzmann model, Transactions of the Japan Society of Mechanical Engineers, Series B 68 (665) (2002) 15–21 (in Japanese).
[6] N. Takada, M. Tsutahara, Proposal of lattice BGK model with internal degrees of freedom in lattice Boltzmann method, Transactions of the Japan Society of Mechanical Engineers, Series B 65 (629) (1999) 92–99 (in Japanese).
[7] S. Chen, G.D. Doolen, Lattice Boltzmann method for fluid flows, Annual Review of Fluid Mechanics 30 (1998) 329–364.

[8] C.K.W. Tam, J.C. Webb, A study of the short wave components in computational acoustics, Journal of Computational Physics 107 (1993) 262–281.
[9] C.K.W. Tam, Computational aeroacoustics: Issues and methods, AIAA Journal 33 (10) (1995) 1788–1796.
[10] J. Smagorinsky, General circulation experiments with the primitive equations, Monthly Weather Review 91 (3) (1963) 99–164.
[11] S. Hou, J. Sterling, S. Chen, G.D. Doolen, A lattice Boltzmann subgrid model for high Reynolds number flows, Fields Institute Communications 6 (1996) 151–166.
[12] A. Michalke, On the inviscid instability of the hyperbolic-tangent velocity profile, Journal of Fluid Mechanics 19 (1964) 543–556.
[13] M. Hiraishi, M. Tsutahara, Outflow boundary condition for numerical simulation of aerodynamic sound by the finite difference lattice Boltzmann method, in: Proceedings of the 7th JSME–KSME Thermal and Fluids Engineering Conference, CD-ROM, 2008.
[14] C. Bogey, C. Bailly, D. Juve, Numerical simulation of the sound generated by vortex pairing in a mixing layer, AIAA Journal 38 (12) (2000) 2210–2218.
[15] C.D. Winant, F.K. Browand, Vortex pairing: The mechanism of turbulent mixing-layer growth at moderate Reynolds number, Journal of Fluid Mechanics Digital Archive 63 (1974) 237–255.